FORMATION OF LINE PROFILE : SEI METHOD

CHOE, SEUNG-URN, KANG, MIN-YOUNG AND KIM, KYUNG-MEE

Department of Earth Sciences, Seoul National University, Seoul 151-742, Korea

ABSTRACT

We have solved the radiative transfer problem using a Sobolev approximation with an escape probability method in case of the supersonic expansion of a stellar envelope to an ambient medium. The radiation from the expanding envelope turns out to produce a P-Cygni type profile. In order to investigate the morphology of the theoretical P-Cygni type profile, we have treated V_∞, V_{sto}, β(parameters for the velocity field), $\dot{M}$ and ϵ(parameter for collisional effect) as model parameters. We have investigated that the velocity field and the mass loss rate affect the shapes of the P-Cygni type profiles most effectively. The secondarily important factors are V_∞, V_{sto}. The collisional effect tends to make the total flux increased but not so much in magnitude. We have infered some physical parameters of 68 Cyg, HD24912, and ξ persei such as V_∞, $\dot{M}$ from the model calculation, which shows a good agreement with the observational results.

Key Words : P-Cygni profile: radiative transfer: Sobolev approximation: escape probability

I. INTRODUCTION

It is important to analyze the observational emission and absorption lines in star and interstellar medium systems. The P-Cygni type line profile is observed in a single star system with an expanding atmosphere. The P-Cygni type profile is variable and depends on the physical conditions of the system. Castor(1970) has obtained expressions for the emergent line profile for a radially expanding envelope. He has used escape probabilities to calculate the line source function. If the envelopes are not optically thin, it is necessary to solve the formidable line transfer equation in the moving medium. Sobolev has developed a method for solving such problems based on neglecting the intrinsic line width relative to the Doppler displacement. With this method Sobolev has defined photon escape probabilities which can be used in the equations of statistical equilibrium of the atomic level populations. Theoretical P-Cygni profiles are calculated by means of a comoving-frame formalism and compared to those obtained from the Sobolev approximation (Hamann, 1981). Hamann pointed out that the error in the sobolev approximation mainly arises from the treatment of the "formal integral", but less from the approximated source function. In case that the stellar envelope is not a spherical symmetry, the radiative transfer can be solved by a generalized Sobolev method which has been developed by Rybicki and Hummer(1978). This method can be applied to the three-dimensional flows with non-local radiative coupling. Hempe(1982) and Baade(1986) developed the computer code for solving the non-spherical, multidimensional radiative transfer problem. Hempe used the escape probability method to calculate the line source function in a two level approximation. In a multilevel analysis Baade(1986)investigated the validity of the two level approximation. In this study, we use the Sobolev approximation as a basic theoretical method and use the computer code developed by Baade. We want to investigate the formation and variation of the line profile theoretically for some models.

We have solved the radiative transfer equation in the SEI(Sobolev with Exact Integration) method (Hempe, 1982 and Kyung-Mee Kim, 1994). We calculated the line profiles changing the parameters - velocity distribution in the velocity field, the mass loss rate of the star, the ratio of collisional to total de-excitation rates from the upper level, and so on. Then we examined the application of the theoretical model to the real system with comparing the theoretical line profiles with the observational line profiles. We explain the possible conditions of the Sobolev

approximation, the radiative transfer equation and the escape probability in the system the conditions can be applied in at section II. We deal with the model calculation at section III and the results of the calculated line profiles from theoretical model at section IV. Then we have finally compared the observational results with the model calculated results, and examined the results and discussed the problems at section V and VI respectively.

II. THEORY

The theory of the radiative transfer is important because photons from a star have astophysical informations for the media they passed through. But, yet the limitted approximation is used in description for the stellar wind model. The radiative transfer problem can be solved by a generalized Sobolev method for three-dimensional flows with non-local radiative coupling, which has been developed by Rybicki and Hummer(1978).

It is difficult to find the formal solution of the radiative transfer equation in the moving medium. Using an appropriate condition the formal solution can be simplified. In case of the large velocity gradient in the medium, the Sobolev approximation can be used.

The transfer equation for a two-level atom in a three-dimensional moving medium has been discussed in detail by Rybicki(1970). It can be written

$$\vec{n} \cdot \nabla I(\vec{r}, \vec{n}, \nu) = -\kappa(\vec{r})\phi[\nu - \frac{\nu_0}{c}\vec{n} \cdot \vec{v}(\vec{r})][I - S] \tag{1}$$

$I(\vec{r}, \vec{n}, \nu)$ is the specific intensity at point $\vec{r}$ in direction defined by the unity vector $\vec{n}$ and at frequency ν, and $\vec{v}(\vec{r})$ is the material velocity field. The quantity

$$\kappa(\vec{r}) = \frac{h\nu_0}{4\pi}B_{12}n_1(\vec{r}) \tag{2}$$

is the integrated line opacity, where ν_0 is the line-center frequency, B_{12} is the Einstein coefficient, and n_1 is the population of the lower level. The line profile function $\phi(\vec{r}, \nu)$ has the frequency normalization

$$\int_0^\infty \phi(\vec{r}, \nu)d\nu = 1 \tag{3}$$

For complete redistribution, the source function is

$$S(\vec{r}) = [1 - \epsilon(\vec{r})]\bar{J}(\vec{r}) + \epsilon(\vec{r})B(\vec{r}) \tag{4}$$

where ϵ is the ratio of collisional to total de-excitation rates from the upper level. B is the Plank function at frequency ν_0 and local electron temperature at point $\vec{r}$. The integrated mean intensity is defined as

$$\bar{J}(\vec{r}) = \frac{1}{4\pi}\int d\Omega \int_0^\infty d\nu\phi[\nu - \frac{\nu_0}{c}\vec{n} \cdot \vec{v}(\vec{r})]I(\vec{r}, \vec{n}, \nu) \tag{5}$$

The formal solution of the transfer equation (2-1) can be written for the intensity at an arbitrary point $\vec{r}$ and direction $\vec{n}$

$$I(\vec{r}, \vec{n}, \nu) = \int_0^R dl\kappa(\vec{r} - \vec{n}l)\phi[\nu - \frac{\nu_0}{c}\vec{n} \cdot \vec{v}(\vec{r})] \cdot S(\vec{r} - \vec{n}l)$$

$$\times exp\{-\int_0^l dl'\kappa(\vec{r} - n\vec{l'})\phi[\nu - \frac{\nu_0}{c}\vec{n} \cdot \vec{v}(\vec{r} - n\vec{l'})]\}$$

$$+ I_\nu^{inc}exp\{-\int_0^R dl'\kappa(\vec{r} - n\vec{l'})\phi[\nu - \frac{\nu_0}{c}\vec{n} \cdot n\vec{u}(\vec{r} - n\vec{l'})]\} \tag{6}$$

The variable of integration l is the distance backwards along the ray passing through $\vec{r}$ with direction $\vec{n}$ (see Fig.1).

When the velocity gradients in the medium are sufficiently large, the (6) equation simplifies. The effect of a large velocity gradient can be seen in the formal solution(6). The argument of the profile function ϕ becomes a function
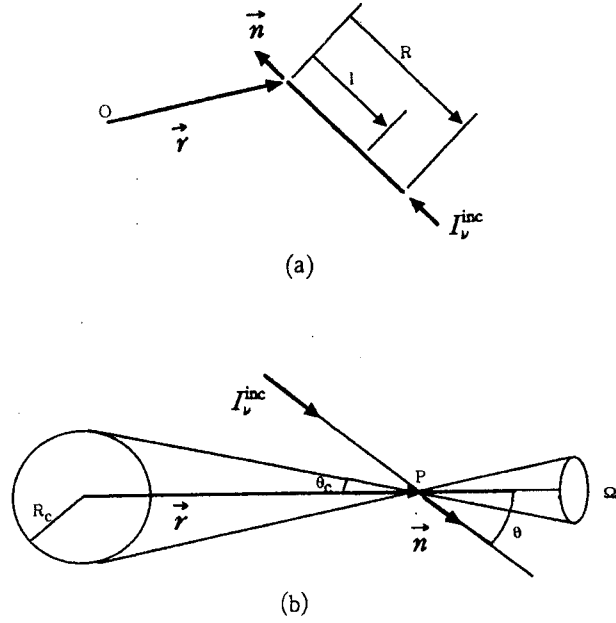
(a)

(b)

Fig. 1. (a) Geometry of variables appearing in the formal solution, eq.(6) ; (b) geometry of the variables entering the calculation of $\bar{J}(\vec{r})$ for a single surface.

of the distance along the ray, and because the profile function is typically very narrow, it behaves like a δ-function in the variable l (or l'). this gives the intensity field within the medium a very simple behavior : Along a given ray the intensity at frequency ν does not change at all, except at certain discrete resonance points, where the material has just the right Doppler shift to allow it to absorb and emit at frequency ν. These point occur wherever the line-of-sight velocity $v_l \equiv \vec{v} \cdot \vec{n}$ satisfies the resonance condition

$$\frac{\nu - \nu_0}{\nu_0} = \frac{v_l}{c} \tag{7}$$

which is found by setting the argument of ϕ equal to ν_0 . Therefore, the problem of determining the intensities reduces to the simpler one of determining the variation of intensity in the neighborhood of a single resonance point. This is the essence of the Sobolev approximation. The validity of the above physical picture depends on the sharpness of the resonance region. Its width Δl can be estimated by assuming that the gradient of v_l is constant over the region. Then differentiation of equation (7)

$$\Delta l = \frac{c}{\nu_0} \frac{\Delta \nu}{|\frac{dv_l}{dl}|} \tag{8}$$

where $\Delta \nu$ is the width of the profile function. Let us estimate $|\frac{dv_l}{dl}| \approx \frac{v_0}{l_0}$, where v_0 is a typical velocity and l_0 is a typical length scale in the medium. Assuming that the line width is due to Doppler broadening, then $\Delta \nu = \nu_0 \frac{u_{th}}{c}$, where u_{th} is the thermal(plus turbulent) velocity. It follows that

$$\frac{\Delta l}{l_0} \approx \frac{u_{th}}{v_0} \tag{9}$$

Therefore, the resonance regions will be relatively sharp when the macroscopic velocities are much larger than thermal ; for this reason the Sobolev approximation is sometimes called the supersonic approximation.

It is clear from the preceding that it is of crucial importance for the Sobolev approximation to locate the resonance points along each ray. A convenient way of representing these locations is through the concept of velocity surfaces.

There are two types of velocity surfaces of particular utility, the common-direction velocity surfaces and the common-point velocity surfaces. The common-direction(CD) velocity surfaces are defined as follows : Consider all rays passing through the medium that have the same direction as would be seen by a distance observer. In the multiple intersection case another kind of velocity surface can be defined as follows : Consider all rays passing through a point $\vec{r}$, and determine along each ray of direction $\vec{n}$ all points $\vec{r'}$ in resonance with $\vec{r}$, that is, such that the line-of-sight velocity is the same at $\vec{r}$ and $\vec{r'}$:

$$\vec{n} \cdot \vec{v}(\vec{r}) = \vec{n} \cdot \vec{v}(\vec{r'})$$

All such points $\vec{r'}$ line on a two-dimensional surface, which must pass through $\vec{r}$, since $\vec{r'} = \vec{r}$ satisfies the equation. The common-point (CP) velocity surfaces are defined as above. Rybicki and Hummer described a prototype velocity law as the inverse power law

$$v(r) = v_0(\frac{r_0}{r})^\alpha, \alpha > 0 \tag{10}$$

for conveniance they took $r_0 = r_c$, the radius of the core, and $v_0 = v(r_0)$. Although there has been a trying to explain the stellar wind theoretically, the processes of the mass loss and accelerating the stellar wind have not been described exactly, yet. So, we assumed the velocity distribution emperically in the examination of the line profiles. Che et al.(1983) used the velocity law given by

$$v(r) = v_\infty(1 - \frac{R}{r})^{\frac{1}{2}} \tag{11}$$

where, r is the distance from the star, R is the radius of the star, and v_∞ is the terminal velocity. This equation represents the process that the wind accelerated near the star reaches its terminal velocity within a few star radii. Hamann(1981) represented the velocity field as following in his paper discussing on the validity of the Sobolev Approximation.

$$v(r) = v_\infty(1 - \frac{b}{r})^\beta \tag{12}$$

where b is fixed by the choice of the minimum velocity $v(r = 1) = 0.01v_\infty$. The parameter β is set either to 0.5 or 2. The first case (square-root-law) corresponds roughly to the result of the stellar wind theory by Castor et al.(1975) and was often adopted in former investigation. This velocity law has a steep gradient near the photosphere. In the law with $\beta = 2$, as the other extreme, the star has a very shallow gradient.

III. MODEL CALCULATION

We have used the Sobolev approximation as a basic theoretical method and have used the computer code developed by Baade(1993). We have rearranged the code to a single star system. The point of this study is to investigate the formation and variation of the line profile theoretically through the model calculation. We have solved the radiative transfer equation in the SEI (Sobolev with Exact Integration) method. We have calculated the line profiles with changing the condition of the system, e.g., velocity distribution in the velocity field, the mass-loss rate of the star, the ratio of collisional to total de-excitation rates from the upper level, and so on.

It is the intensity of emergent radiation flux that we want to get, which forms the profile. It can be changed with the various frequency. It is calculated through the integration of the radiative transfer equation. In the star-centered coordinate, the intensity is calculated by setting the net-point-structures in the integrating range for the frequency, distance from the star, and azimuth on the celestrial sphere. Whenever the calculation is accomplished in each net-point, the source function is interpolated. To calculate the P-Cygni type line profile in the expanding envelope of the stars which have strong stellar winds, the model parameters have been adopted in table 1.

Table 1. The model parameters of two models

Model 1		Model 2	
R	$15R_\odot$	R	$10R_\odot$
V_∞	$2000kms^{-1}$	V_∞	$3500kms^{-1}$
M	$1 \times 10^{-7}M_\odot yr^{-1}$	M	$2 \times 10^{-6}M_\odot yr^{-1}$

We adopted the parameters of the Model 1 from Cator(1970) and those of Model 2 from Shull(1993). To envestigate the change of line profile, the various physical parameters have been adopted such as V_∞, V_{sto}, β, $\dot{M}$,and ϵ in the reasonable range. Each parameters have been included in the equations of the calculation:

Radiation flux:

$$\frac{F(x)}{F_c} = \frac{\int_0^\pi \int_0^R I(x,P,\phi)rdrd\phi}{\int_0^\pi \int_0^{R_c} I_c(x,P,\phi)rdrd\phi} \tag{13}$$

The integral equation:

$$I(\nu,P,\phi,z) = \int_0^{\tau_{max}} S(P,\phi,z)exp[-\tau(\nu,P,\phi,z)]dz + \begin{cases} I_c exp[-\tau_{max}(\nu,P,\phi)] & \text{if } P \leq R_{star} \\ 0 & \text{if } P > R_{star} \end{cases} \tag{14}$$

$$\tau(\nu,P,\phi,z) = \int_z^{z_{max}} \kappa(r)\phi_\nu dz \tag{15}$$

Source function:

$$S(\vec{r}) = \frac{(1-\epsilon)\beta_c I_c + \epsilon B}{\epsilon + (1-\epsilon)\beta} \tag{16}$$

Escape probability:

$$\beta(r) = \frac{1}{2} \int_{-1}^1 d\mu \frac{(1-e^{-\tau_s})}{\tau_s} \tag{17}$$

$$\beta_c(r) = \frac{1}{2\pi} \int_{\mu_c}^1 \int_0^\pi d\phi d\mu \frac{(1-e^{-\tau_s})}{\tau_s} \tag{18}$$

$$\tau_s = \tau_0 \frac{r}{V(r)}[1 + \mu^2(\frac{d\ln V(r)}{d\ln r} - 1)]^{-1} \tag{19}$$

Velocity field:

$$V(r) = V_\infty(1 - \frac{R_{star}}{r})^\beta \tag{20}$$

IV. CALCULATION RESULTS

(a) Effects of the Various Final Velocities and Stochastics Velocities

The terminal velocity of a stellar wind, V_∞ is defined as the velocity of outflowing matter at large distances from the star, where it is no longer experiencing significant acceleration but is not yet interaction significantly with the interstellar medium (Prinja & Barlow, 1990). Terminal velocities are needed for the determination of mass-loss rate, because $\dot{M} \propto V_\infty^2$ for the UV resonance line profiles or $\dot{M} \propto V_\infty$ for the radio measurements of the free-free random from the winds. Since the time of the first large-scale ultraviolet spectroscopic survey of the mass-loss characteristics of luminous OB stars(Snow and Morton, 1976), the terminal velocity of a stellar wind has normally been obervationally defined as the modulus of the largest negative velocity seen in absorption in the P-Cygni profiles of UV resonance lines. In case of a large final velocity, if the stellar wind accelerates with the same tendency, the velocity is larger at each points than that in case of a small final velocity. So, the effect of a Doppler displacement comparatively is larger. As the line forms in a broad range from the center of the line frequency, the absorption part is displaced to the short wavelengh and the emission part is placed to the long wavelengh. Surely, each line width is broadend(Fig.2).

The stochastic velocity includes both effects of the thermal velocity and the turbulence velocity. As the stochastic velocity increases, the line profile has the more rounded shape and a tendency for broadening the absorption part. The emission peak is shifted to the direction of a long wavelengh, i.e., the higher positive velocity and the absorption part is shifted to the direction of the short wavelength, i.e., the higher negative velocity. So, the flux at the central
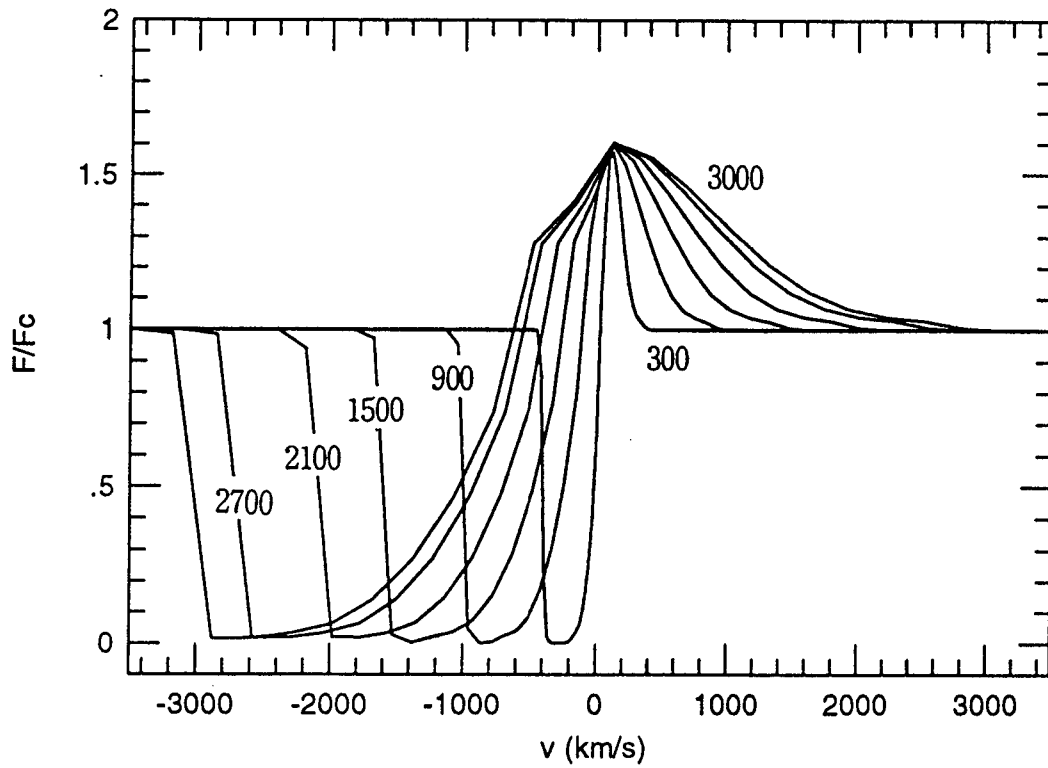
Fig. 2. The change of line profile for the various final velocity, V_∞. The line width broadens, as the V_∞ increases. $V_\infty = 3000$, $2700, 2100, 1500, 900, 300 km/s$
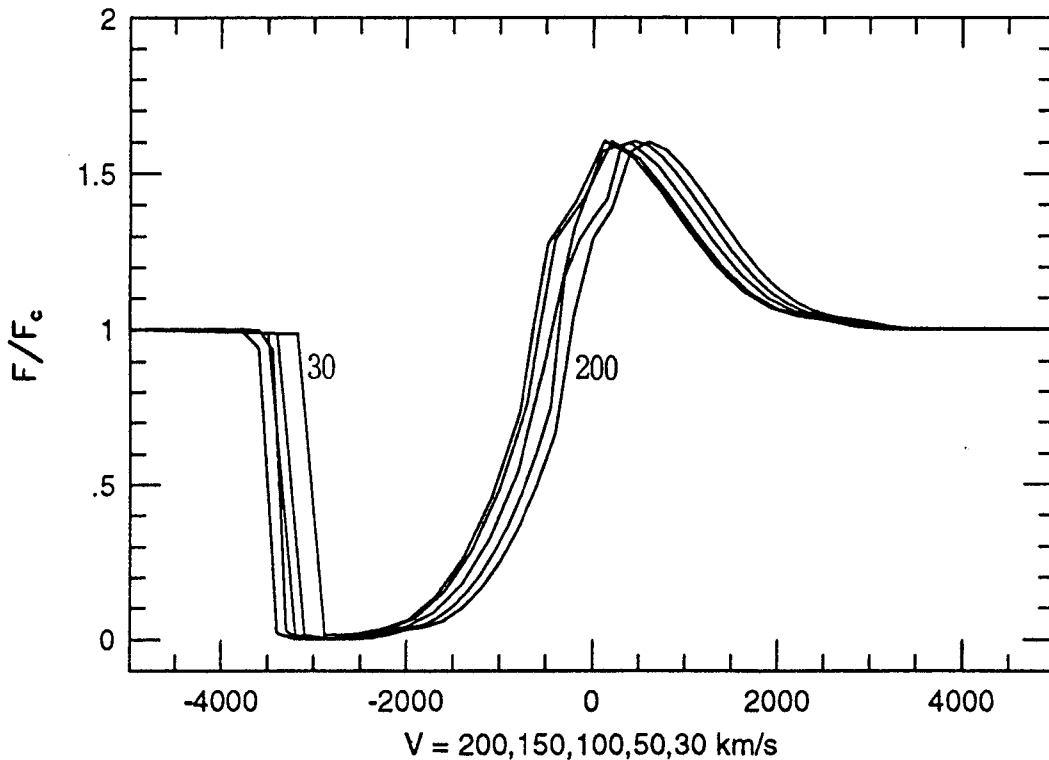

Fig. 3. The change of line profile for the stochastic velocity, V_{sto}. As the V_{sto} increases, the line width broadens. The tendency is large for the absorption part. $V_{sto} = 200, 150, 100, 50, 30 km/s$
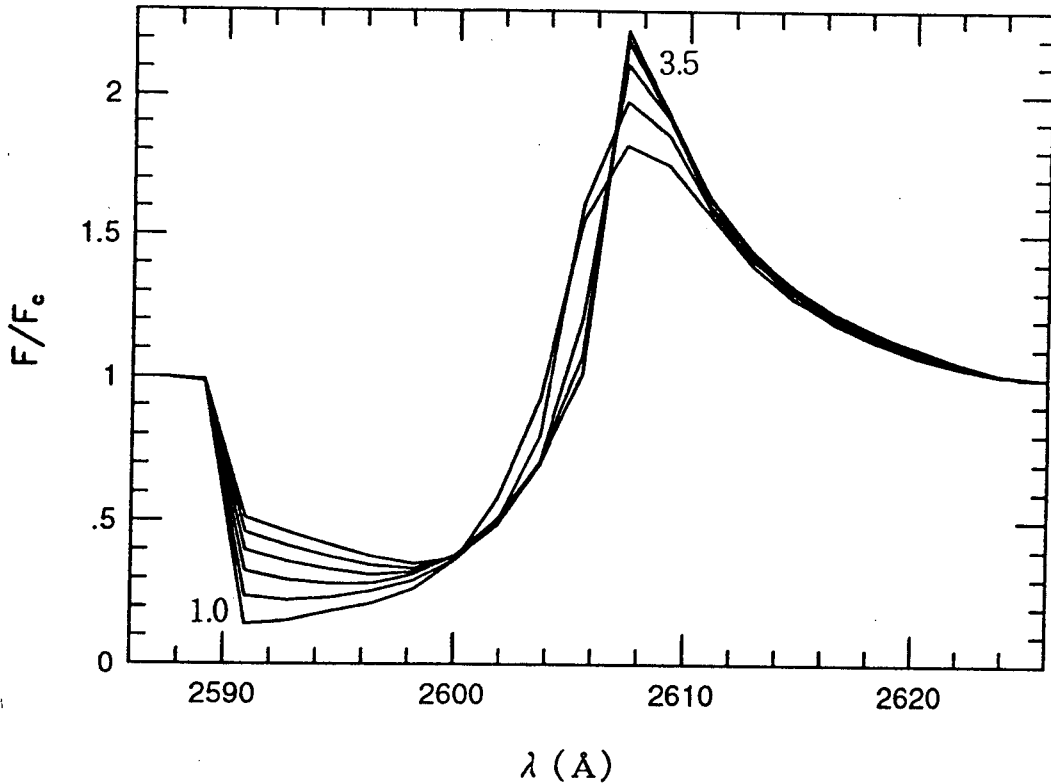
Fig. 4. The change of line profile with the increasing β in the model 1; $V_\infty = 2000km/s$, $\dot{M} = 10^{-7}M_\odot/yr$. In case of $\beta = 3.5$, the line has a maximum emission peak. $\beta = 3.5, 3.0, 2.5, 2.0, 1.5, 1.0$

wavelengh which has a zero velocity decreases. This result is the same as that of Hamann(1981). The peak intensity in the emission part has no change at al(Fig.3).

(b) Effects of Velocity Field

The velocity field in the calculation is given from the eq.(20) where β is changed in a range $\beta = 0.5 \sim 3.5$. For the larger value of β, the line width is likely to be narrower and the emission peak to be higher. When $\beta = 0.5$, the whole line profile is smooth. The emission part is broad and the absorption part is also broad but deeper. The left side of the absorption part connected to the continuum has a large gradient(Fig.4). The flux has its maximum value near the central wavelength. The larger β is, the higher the maximum intensity is and the line profile becomes sharper, and the absorption part has a tendency to be shallow. Especially, as the left part of the absorption part connected to the continuum has the gradients decreasing, the depth of the absoprtion part becomes deeper. This result is the same as that of Hamann's calculation(1981). He calculated the line profile with changing the velocity field and line opacity. According to his calculation, the optical thick line, opacity of which is very large, has a deep absorption part and no difference although the velocity field have some changes. But, the unsaturated line, opacity of which is comparatively small, shows the same results as showed in Fig.4. Figure 5 has not much changes in the absoption parts and the emission peak is higher than that in Fig.4. As the mass-loss rate increases, the line opacity proportional to it increases also. Therefore Fig.5 is the same as the case of the Hamann's optically thick line.

(c) Effects of Mass-Loss Rate

The line profile is also affected by the opacity of the matter which the ray passes through. In the Sobolev approximation, the stellar mass-loss rate with the velocity distribution is the important factor to form the line profile. As the opacity is proportional to the mass-loss rate, the mass-loss rate is adopted as the parameter of a line
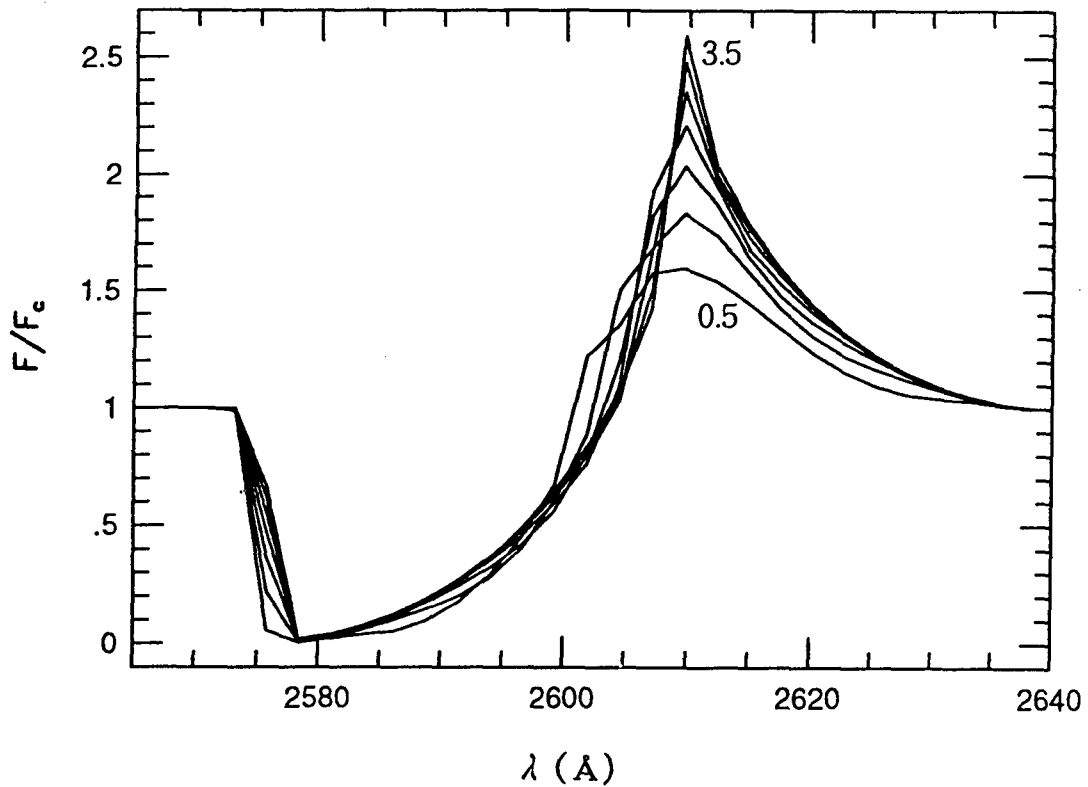
Fig. 5. The change of line profile with the increasing β in the model 2; $V_\infty = 3500km/s$, $M = 2 \times 10^{-6}M_\odot/yr$. In case of $\beta = 3.5$, the line has a maximum emission peak. $\beta = 3.5, 3.0, 2.5, 2.0, 1.5, 1.0, 0.5$

calculation, instead of the opacity. The mass-loss rate strongly affects the absoprtion and emission parts(Fig.6). In the range of $10^{-7} \sim 6 \times 10^{-8}M_\odot yr^{-1}$, the emission parts have almost no change but the deep parts of the absorption lines have a tendency to be shallow as the mass-loss rate decreases. In the range of $4 \times 10^{-8} \sim 10^{-8}M_\odot yr^{-1}$, the line profiles change a lot in their shapes. The radiation flux decreases and the absoption part becomes weak, because the opacity is considered to be lower. Fig.7 shows the flux change for the various mass-loss rates in the O type star model. Compared to Fig.6, it has not showed such a change. In the range of $10^{-6} \sim 4 \times 10^{-7}M_\odot yr^{-1}$, the emission parts are not much changed, but in the range of $2 \times 10^{-6} \sim 10^{-7}M_\odot yr^{-1}$, they show small change in their shapes. Fig.8 shows a tendency for the flux variation. In case of Model 1, as the mass-loss rate increases, the maximum values of the emission part increase slowly with a factor of 1.2, and the minimum values of the absorption line decrease rapidly with a factor of 0.2. Whereas, in case of Model 2, this tendency is not much. The factors of the flux is much smaller than those of Model 1.

(d) Effect of the Collisional Effect Parameter

The whole line flux increases as the parameter ϵ increases. Fig.9 gives the similar tendencies of the line profiles in two models. In the range of $\epsilon = 0 \sim 10^{-6}$, the line profiles have no change. For the larger ϵ, the flux increases at each point, then the line profiles are shifted to higher intensity. In the Model 2, the absorption parts show the difference shape. According to Rybicki and Hummer(1978), the source function depends on ϵ which affects the line profile. Castor(1970) approximated the source function and calculated the line profile with the various values of ϵ. As ϵ becomes larger, the whole flux increases as a whole and the absorption part becomes weaker.
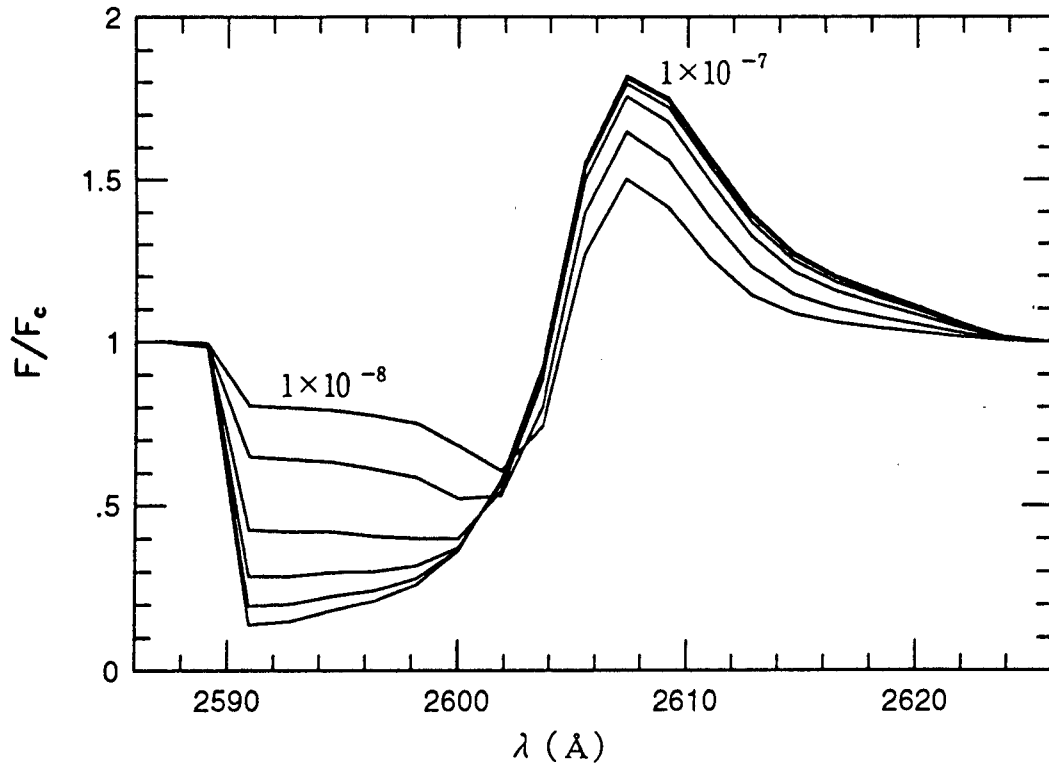
Fig. 6. The change of the line profile for mass-loss rate. $\dot{M} = 1 \times 10^{-7}, 8 \times 10^{-8}, 6 \times 10^{-8}, 4 \times 10^{-8}, 2 \times 10^{-8}, 1 \times 10^{-8} M_\odot / yr$
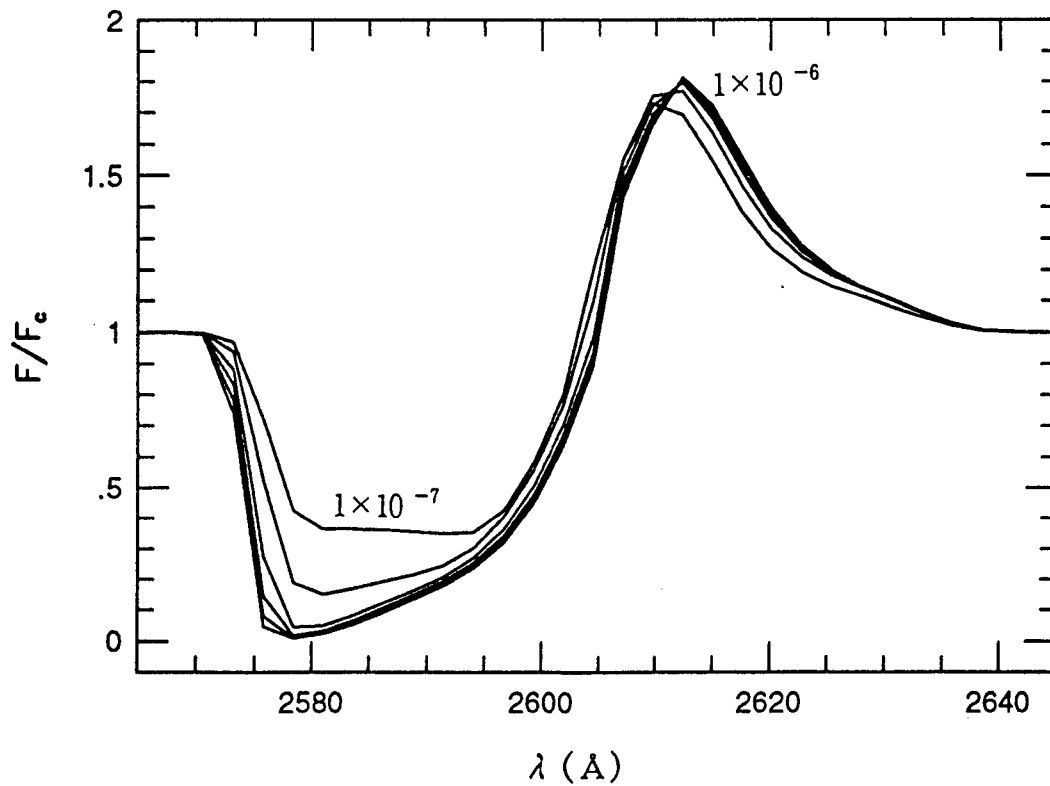

Fig. 7. The change of the line profile for mass-loss rate. $\dot{M} = 1 \times 10^{-6}, 8 \times 10^{-7}, 6 \times 10^{-7}, 4 \times 10^{-7}, 2 \times 10^{-7}, 1 \times 10^{-7} M_\odot / yr$
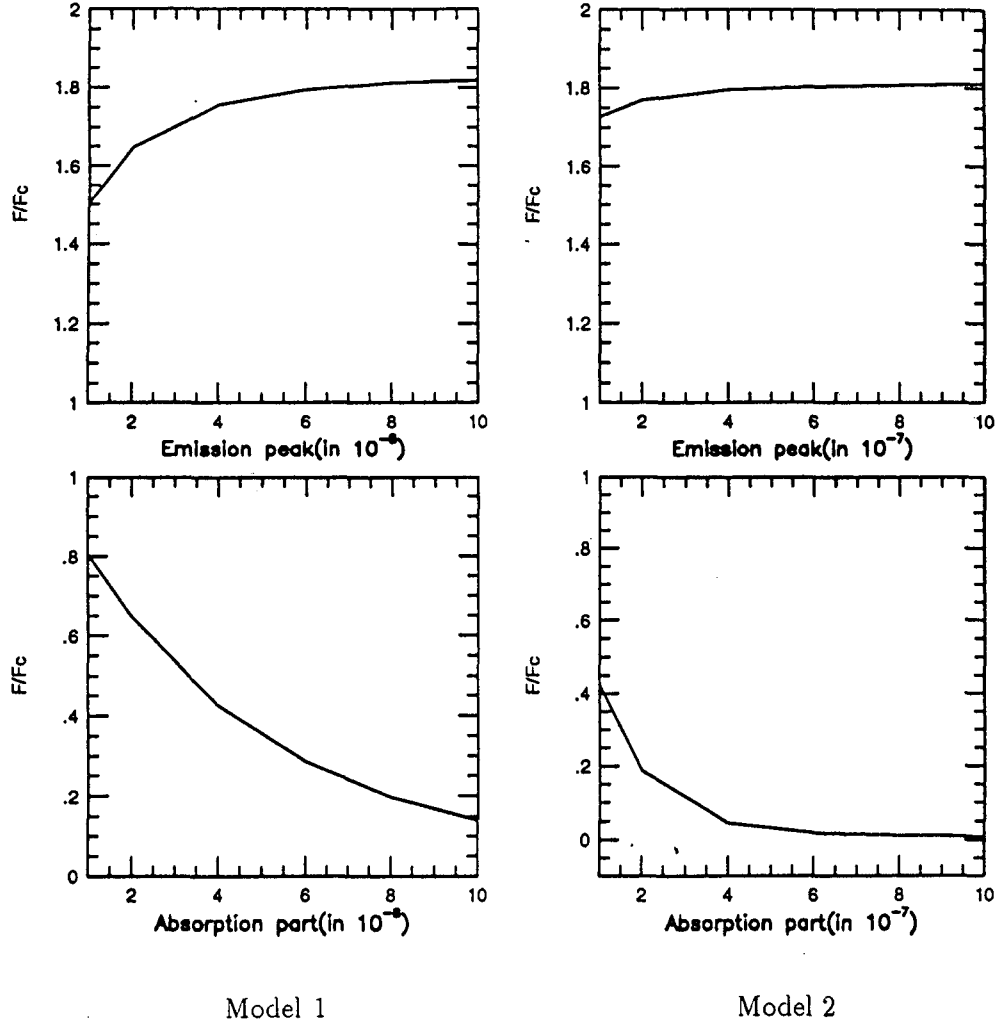
Model 1   Model 2

Fig. 8. The flux variation with different mass-loss rate.

V. COMPARING OBSERVATION WITH MODEL CALCULATION

We have compared the results by the theoretical model calculation to the observations. Three objects are adopted, showing P-Cygni type CIV line profiles in UV region. 68 Cyg is a ordinary O 7.5III type star(Howard and Smith, 1995). The observation estimates the velocity, $V_{max} = 2930kms^{-1}$, which is compared to our model calculation of $V_{\infty} = 3000kms^{-1}$ (Fig.10). Prinzja and Balow(1990) estimated the stellar wind velocity of HD24912, OIII type star; $V_{max} = 2500kms^{-1}$, and $V_{\infty} = 2330kms^{-1}$. We estimate the physical values of $V_{\infty} = 2500kms^{-1}$, $V_{sto} = 300kms^{-1}$, and $\dot{M} = 10^{-6}M_{\odot}yr^{-1}$ (Fig.11). ξ Persei, O 7.5 giant star has been observed to have the P-Cyg profile of CIV line (Henrichs et al., 1994). We estimate $V_{\infty} = 2500kms^{-1}$ and $\dot{M} = 10^{-6} \sim 10^{-5}M_{\odot}yr^{-1}$ (Fig.12).

One of the reason the observed line and calculated line do not match well each other is that CIV line is a doublet. Actually $\lambda = 1548.2\mathring{A}$ and $\lambda = 1550.8\mathring{A}$ lines affect each other complicatedely by scattering and re-emission, because the doublet does not represent as a sum of the two lines. However, in our calculation, we considered the CIV line as a singlet.

VI. CONCLUSION

In order to solve the radiative transfer equation in an expanding medium to which, the Sobolev approximation has been applied, we have assumed the 2 level atom and used the SEI method. To examine the line formation
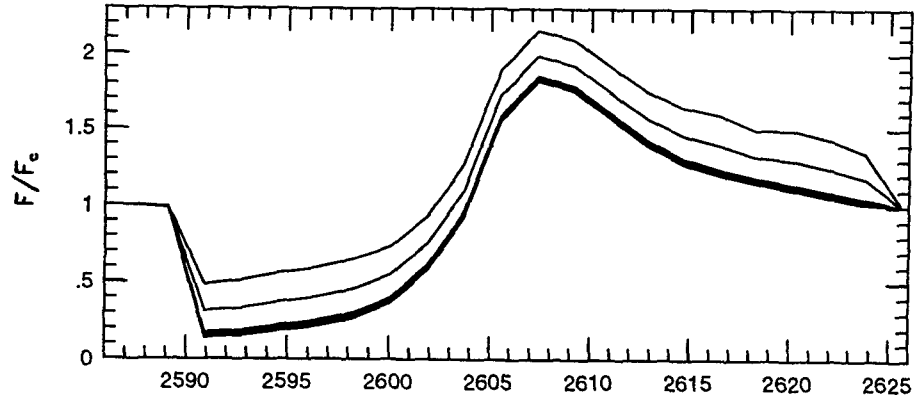
(a)
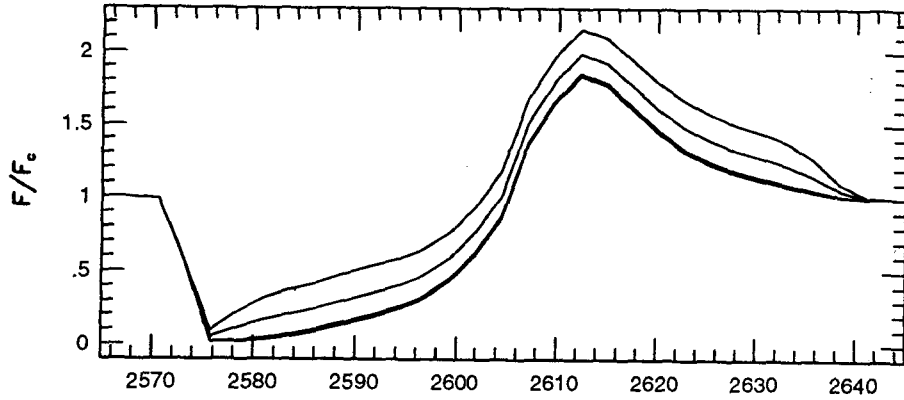
(b)

Fig.9. The change of the line profile with the various ϵ. (a) model 1, (b) model 2. In the range of $\epsilon = 0 \sim 10^{-6}$, the line profile has little change in its shape.

in a single star system theoretically, we adopted the various physical parameters such as the final and stochastic velocities as, the velocity field, the mass-loss rate, and the collisional effect in the adopted two models. It is the velocity field that affects the shapes of the line profile more effectively. The mass-loss rate affects it considerably too. The collisional effect is not much important.

We compared the results of model calculation to the observed CIV line profiles of three objects. We estimated their final velocities and mass-loss rates respectively. For 68 Cygni, $V_\infty = 3000 km s^{-1}$, $\dot{M} = 1 \times 10^{-7} \sim 2 \times 10^{-6} M_\odot yr^{-1}$. For HD24912, $V_\infty = 2500 \sim 2700 km s^{-1}$, $\dot{M} = 1 \times 10^{-6} M_\odot yr^{-1}$. For ξ Persei, $V_\infty = 2500 km s^{-1}$, $\dot{M} = 1 \times 10^{-6} \sim 1 \times 10^{-5} M_\odot yr^{-1}$. The physical values estimated in the model calculation should explain the observed results.
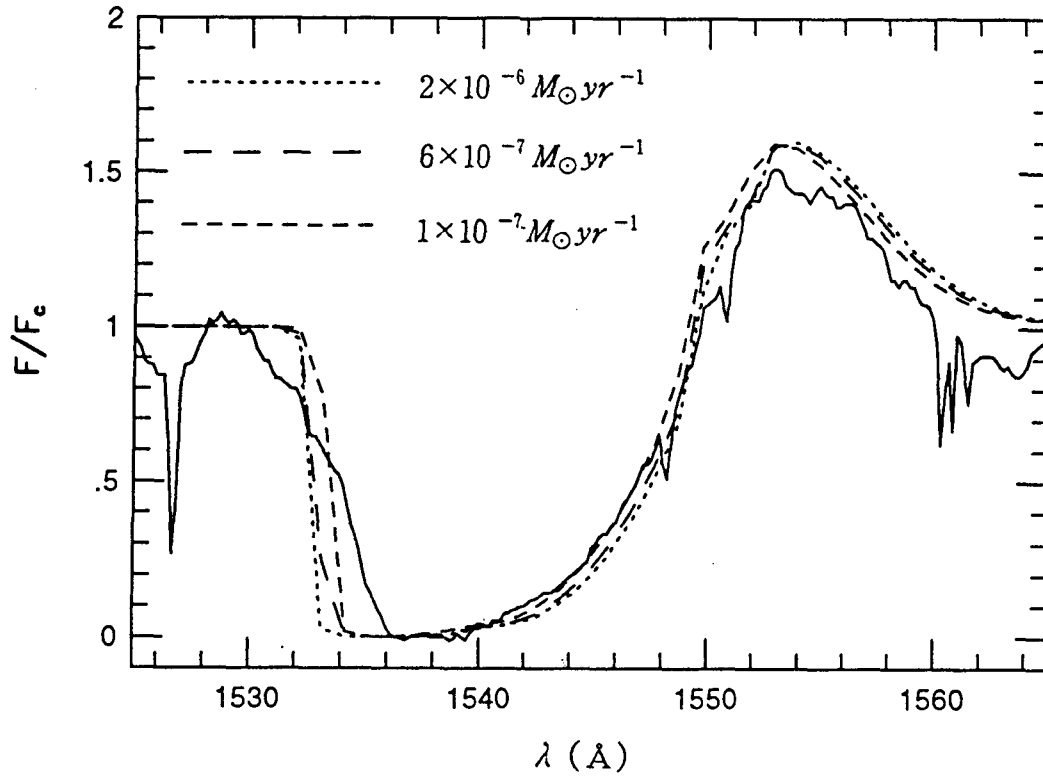
ACKNOWLEDGEMENTS

Fig.10. The observed and calculated CIV ($\lambda = 1550.8\text{Å}$) lines of 68 Cyg. Model calculation estimates the physical values of 68 Cyg star ; $V_\infty = 3000 kms^{-1}$, $V_{sto} = 200 kms^{-1}$, $\dot{M} = 10^{-7} \sim 2 \times 10^{-6} M_\odot yr^{-1}$
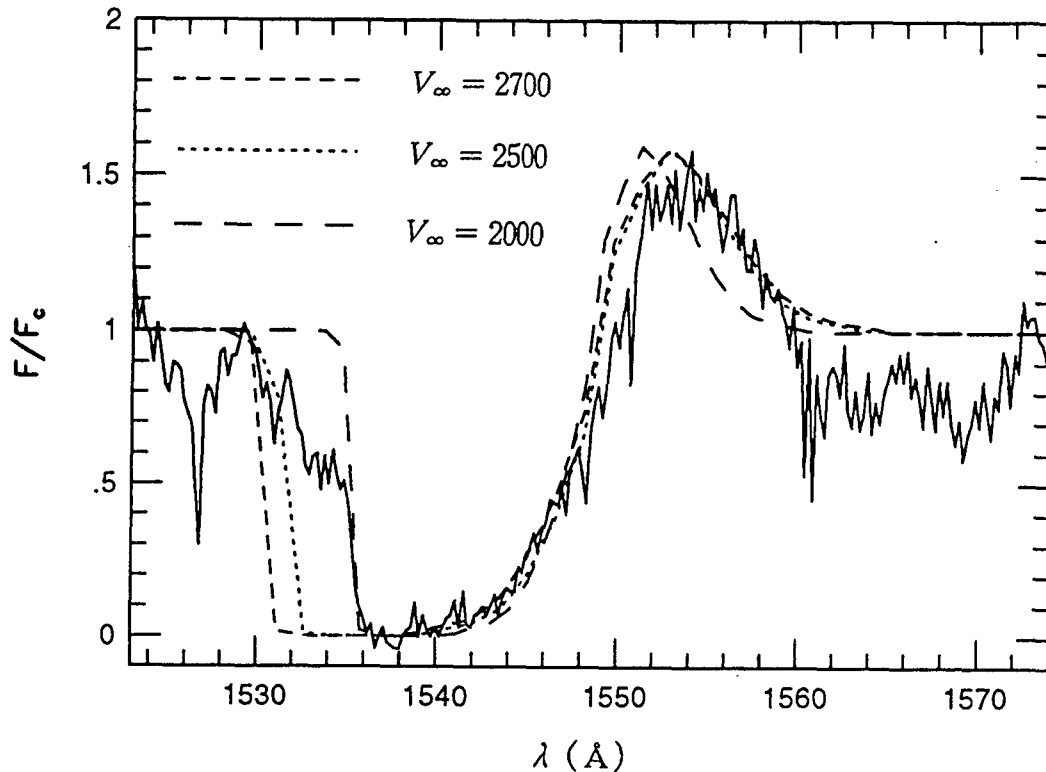

Fig.11. The observed and calculated CIV ($\lambda = 1548.2\text{Å}$) lines of HD24912. Model calculation estimates the physical values of HD24912 ; $V_\infty = 2500 \sim 2700 kms^{-1}$, $\dot{M} = 10^{-6} M_\odot yr^{-1}$

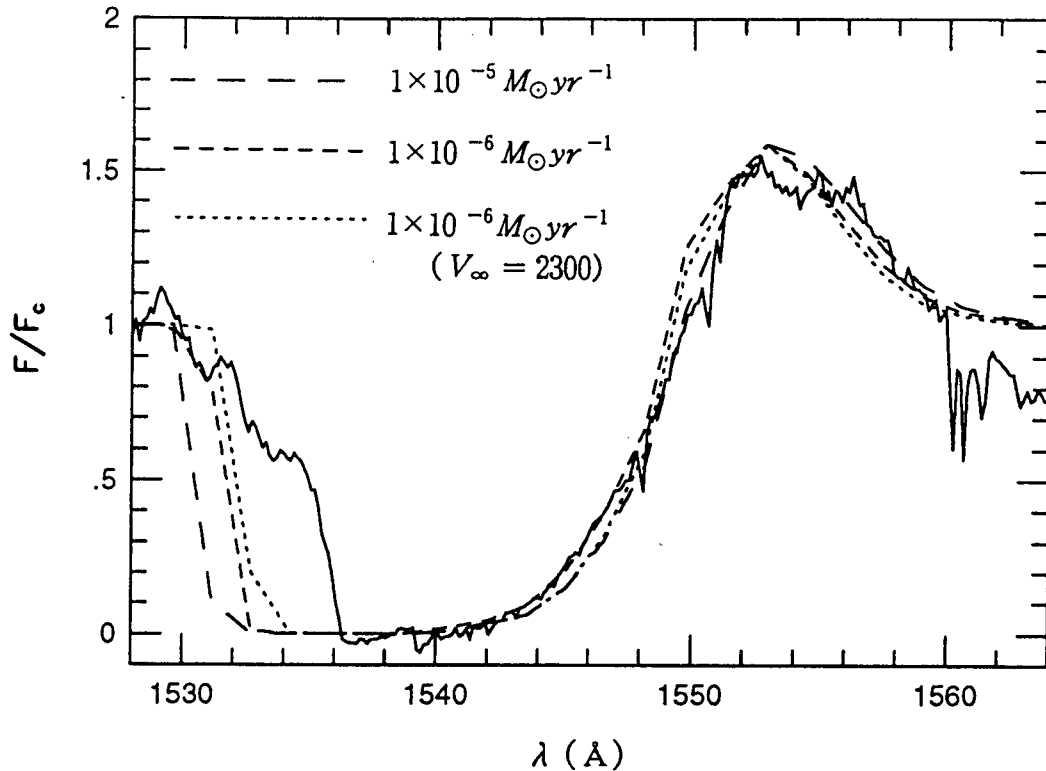**Fig.12.** The observed and calculated CIV ($\lambda = 1548.2\text{Å}$) lines of ξ Persei. Model calculation estimates the physical values of ξ Persei ; $V_\infty = 2500 kms^{-1}$, $\dot{M} = 10^{-6} \sim 10^{-5} M_\odot yr^{-1}$

REFERENCES

Baade, R., 1986, A&A, 154, 145

Baade, R., 1990, A&A, 233, 486

Castor, J. I., 1970, M.N.R.A.S., 149, 111

Che, A., Hempe, K., and Reimers, D., 1983, A&A, 126, 225

Hamann, W. R., 1981, A&A 93, 353

Hempe, K., 1982, A&A, 115, 133

Henrichs, H. F., Kaper, L., and Nichols, J. S., 1994, A&A, 285, 565

Howarth, I. D., Smith, K. C., 1995, ApJ, 439, 431

Mihalas, D., 1978, Stellar Atmospheres, Freeman and Company

Prinja, R. K., Barlow, M. J., 1990, ApJ, 361, 607

Rybicki, G. B., Hummer, D. G., 1978, ApJ, 216, 654

Shull, J. M., 1993, ASP Conf. Ser., 35, Cassinelli et al. eds., p.327

Snow, T. P., Morton, D. C., 1976, ApJS, 32, 429